Exploring the Biological and Theoretical Aspects of Rare Earth Metal Mixed Ligand Complexes: A Synergistic Approach

Jani D.N.[1], Jani D.H.[2]* and Paghadar N.A.[3]
1. Dr. Subhash University, Dr. Subhash Road, Joshipura, Junagadh-362001, Gujarat, INDIA
2. Faculty of Science, Noble University, Bhesan road, Junagadh 362310, Gujarat, INDIA
3. Bhaktakavi Narsinh Mehta University, Junagadh 362310, Gujarat, INDIA
*darshan.jani@nobleuniversity.ac.in; darshanjani09@gmail.com

Abstract
In order to create novel transition metal-based coordination compounds, Schiff bases based on the sulpha drug reacted with various 2-hydroxy-benzaldehyde derivatives. The antibacterial properties and spectroscopic attributes of the synthesized ligands and their heterochelates were extensively examined. The structural characterization of the ligands was accomplished through ^{1}H-NMR, IR, Mass spectrometry, UV-Vis spectroscopy and elemental analysis, while the heterochelates' structures were validated using IR spectroscopy.

In vitro evaluations were conducted to assess the activity of the ligands and heterochelates against Gram +ve bacteria (S. aureus, B. subtilis), Gram -ve bacteria (E. coli, P. aeruginosa) and against fungi A. niger. The findings underscore the promising nature of coordination compounds based on transition metals and highlight the necessity of further exploration in this field.

Keywords: Sulpha Drug, Schiff Base, Transition Metal Complexes, Antimicrobial Study, Antifungal Study.

Introduction

Since many types of bacteria and fungi that are resistant to drugs have emerged globally, which are resistant to antimicrobial agents due to structural mutations, many infectious and contagious diseases have spread in the modern era, necessitating the use of medications to prevent them. Sulfonamides are a well-known type of synthetic drug. They are analogous para-aminobenzoic acid and block an enzyme called dihydropteroate synthetase (DHPTS), which is crucial in the folic acid metabolism of bacterial cells[33,40]. Most sulfa drugs work by preventing bacteria from reproducing, as they inhibit a key enzyme required for producing proteins and nucleic acids within bacterial cells[23,31].

Organic molecules with π-conjugated systems are incredibly versatile, allowing for a variety of substitutions and functions, making them important in biochemistry[35,36] and organometallic chemistry. Sulfonamides with a free amino group are especially easy to modify because of free amine group which opens the door to many biomedical uses[29]. Sulfonamides that include imino or hydrazino-modified groups have also shown to be effective at inhibiting CA isozymes[34]. Imino groups (-CR=N-) are produced when primary aromatic or aliphatic amines condense with aldehydes or ketones to make Schiff bases. The above compounds are known to be adaptable pharmacophores that are essential for a range of pharmacological actions. Their bioactivity is mostly dependent on the azomethine group.

Whether derived from natural or synthetic sources, Schiff bases have shown potent antibacterial, antitubercular, antifungal, antiparasitic, antiviral, antioxidant, anticancer, analgesic and anti-inflammatory qualities[1,3,5]. They are hence widely used and appreciated scaffolds in medicinal chemistry. Whether in their free form or as ligands in metal complexes, Schiff base complexes are regarded as one of the most well-known stereochemical models in main group and transition metal coordination chemistry due to their permeability and structural complexity. Numerous metals from the periodic table, primarily from the d-block, as well as a range of organic ligands, ideally with proven bioactivities, have been explored as a result of the work. As a result of their readily available basic components, ideal synthesis conditions and controllable density, Schiff bases have been shown in numerous studies to be effective binders[4].

Schiff bases made from substituted salicylaldehydes (2-hydroxybenzaldehydes) are proven antibacterial agents[6,17,21,22]. It has been demonstrated that the biological effects of Schiff bases of various sulphonamides are similar[11,16,28]. In commercial medication development, heterocyclic compounds especially those with nitrogen and sulphur atoms are regarded as an essential class[24,25]. Antibacterial[12], antitumor[9], diuretic[37], anti-carbonic anhydrase (anti-CA)[38], hypoglycemic[2], anti-thyroid[16] and protease inhibitor[10] properties are among the many uses for sulphonamides and their Schiff base-derived derivatives. When given as metal complexes, several medications show changed pharmacological and toxicological characteristics.

Effective suppression of carbonic anhydrase (CA) isozymes has also been shown for sulphonamides with imino or hydrazino-modified groups[32]. The biological properties of metal complexes depend on how easily the bond between the metal ion and the ligand can be broken. It is essential to comprehend the coordination behaviour and the interaction between ligands and metals in biological systems. We have

started a program[13-15] aimed at creating and designing different metal-based sulphonamides in order to investigate their structural and biological characteristics, given the varied chemistry of sulphonamides as ligands. Structures containing sulphur are present in many pharmaceuticals and natural products[30], where they serve important functions and exhibit a variety of biological effects[7,8].

Sulphur has been a small, ring-shaped atom for a long time and it is a component of more than 362 FDA-approved drugs that contain nitrogen, oxygen, or sulfur[35]. Sulfones, sulphonamides and molecules with C-S linkages are used to achieve this. In addition to this work, we synthesised two Schiff base ligands derived from 4-Amino-N-(6-methoxypyrimidine-4-yl)benzenesulfonamide and salicyldehyde derivatives (Figure 1). The ligand further used for complexation with molybdenum, tungsten, vanadium and zirconium ions. The suggested complexes' structures are shown in figure 2 and their antibacterial and antifungal properties against *A. niger* fungal species as well as two-Gram positive and two-Gram negative bacterial strains (*B. subtilus*, *S. aureus* and *P. aerugenosa*, *E. coli*) are further examined. The results suggested moderate to significant activity towards the various tested species. The electronic properties of Ligand L_1 and L_2, calculated using DFT at the def2-TZVP level, reveal a HOMO and LUMO energy followed by docking studies.

Material and Methods

All of the raw materials, reagents and solvents used in the research were sourced from a local supplier, were incredibly pure and were used immediately without any further processing. The reaction's progress was assessed using 60 F-254 silica gel plates and Merck pre-coated aluminum sheets in thin-layer chromatography (TLC). An optimized solvent system was used as the mobile phase and results were visualized under iodine vapor and ultraviolet light. An AvanceNeo Ascend 400 MHz equipment was used to record 1H-NMR spectra in DMSO-d6 solution at a neighboring research center and a Perkin-Elmer spectrometer operating in the 4000–400 cm^{-1} range was used to capture infrared (IR) spectra. Additionally, FT-IR spectra were measured using a Nicolet-400D spectrophotometer equipped with a KBr pellet method. The UV spectra were collected using the UV-Vis spectrophotometer V-750.

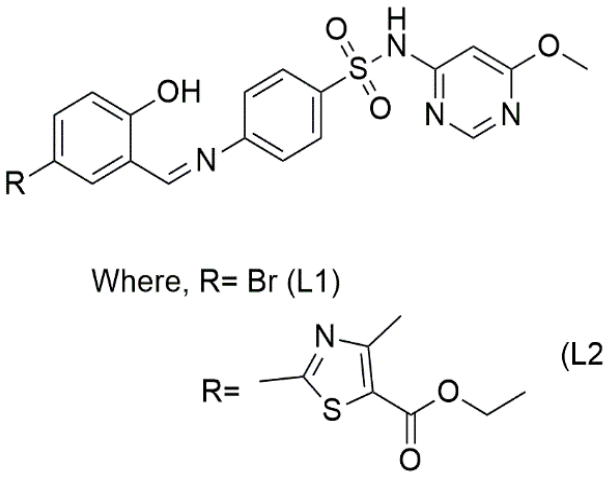

Figure 1: Proposed structure of Ligand

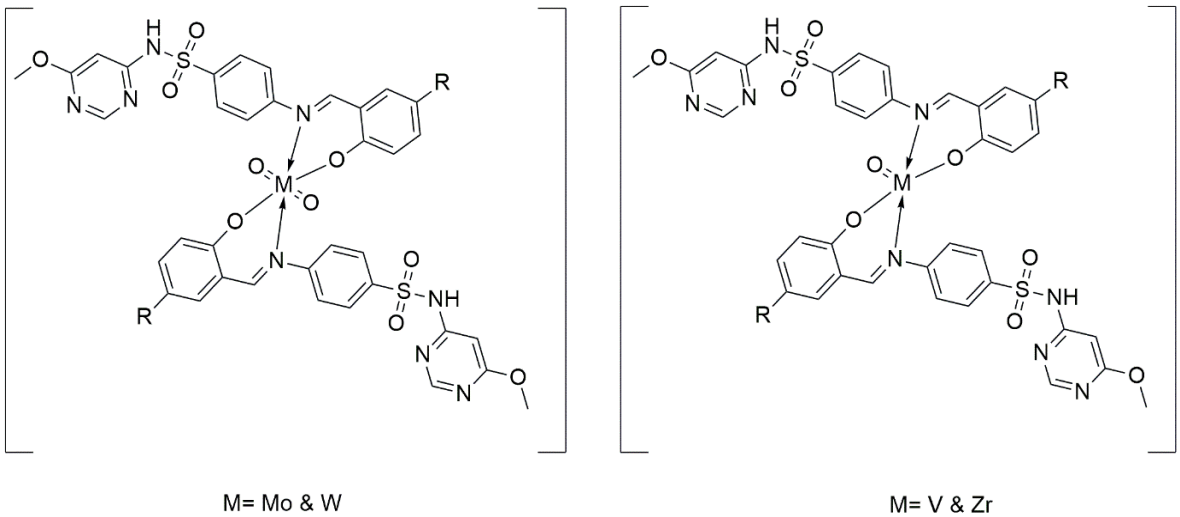

Figure 2: Proposed structure of Heterochelates

General procedure of ligands (L_1 and L_2): By reacting 10 mmol of 4-Amino-N-(6-methoxypyrimidine-4-yl) benzenesulfonamide with an equimolar amount of 5-bromo-2-hydroxybenzaldehyde (L_1) and ethyl-2-(3-formyl-4-hydroxyphenyl)-4-methylthiazole-5-carboxylate (L_2) in methanol while stirring continuously at 35°C, ligand L_1 and L_2 were synthesized. Using a hexane/ethyl acetate (7:3) combination as the mobile phase, thin-layer chromatography (TLC) was used to track the reaction's progress and verify that all of the starting ingredients had been consumed within 30 minutes. After everything was finished, the solid product was separated by filtering, completely cleaned with ethanol, dried at 60°C and then stored for later use.

General procedure of heterochelates: A basic procedure was used to manufacture and separate each heterochelate. Warm metal salt solution made in DMF was added drop by drop to the corresponding ligand solution in 1:2 metal to ligand molar ratios while being continuously stirred. Following four hours of heating at 70˚C, the mixture was allowed to cool overnight at room temperature. A densely colored product emerged after cooling at room temperature and was allowed to dry in desiccators.

Physical and Spectral Data of ligands and its heterochelates

L_1: M.F.-$C_{17}H_{16}N_4O_4S_2$; yield 89%; M. W. 463.31; Orange color; FT-IR (KBr, cm^{-1}); 3360 ν(–OH), 1593 ν(C=N), 1153 ν(SO_2); ^{1}H-NMR (400MHz, DMSO-d^6); δ(ppm); 3.85 (3H,s,-OCH_3); 12.40 (1H,s,-CH); 6.37-8.91 (9H,c,Ar-H); Elemental Analysis Found (%) C, 46.64; H, 3.22; N, 12.07 Calculated for $C_{17}H_{16}N_4O_4S_2$ C, 46.66; H, 3.26; N, 12.09.

[$(L_1)_2MoO_2$]: M.F.-$C_{36}H_{28}Br_2MoN_8O_{10}S_2$; yield 79%; M.W. 1052.55; Orange; Elemental Analysis Found (%) C, 41.06; H, 2.65; N, 10.64; Mo, 9.15; Calculated for $C_{36}H_{28}Br_2MoN_8O_{10}S_2$; C, 41.08; H, 2.68; N, 10.65; Mo, 9.12.

[$(L_1)_2WO_2$]: M.F.-$C_{36}H_{28}Br_2N_8O_{10}S_2W$; yield 77%; M.W 1140.43; Brown; Elemental Analysis Found (%) C, 37.89; H, 2.45; N, 9.80; W, 16.14; Calculated for $C_{36}H_{28}Br_2N_8O_{10}S_2W$; C, 37.91; H, 2.47; N, 9.83; W, 16.12.

[$(L_1)_2VO$]: M.F.-$C_{36}H_{28}Br_2N_8O_9S_2V$; yield 81%; M.W 991.54; Brown; Elemental Analysis Found (%) C, 43.59; H, 2.83; N, 11.27; V, 5.17 Calculated for $C_{36}H_{28}Br_2N_8O_9S_2V$; C, 43.61; H, 2.85; N, 11.30; V, 5.14.

[$(L_1)_2ZrO$]: M.F.-$C_{36}H_{28}Br_2N_8O_9S_2Zr$; yield 76%; M.W. 1031.82; Brown; Elemental Analysis Found (%) C, 41.88; H, 2.71; N, 10.82; Zr, 8.88; Calculated for $C_{36}H_{28}Br_2N_8O_9S_2Zr$; C, 41.91; H, 2.74; N, 10.86; Zr, 8.84.

L_2: M.F.-$C_{25}H_{23}N_5O_6S_2$; yield 81%; M. W. 553.61; Pink color FT-IR (KBr, cm^{-1}); 3360 ν(–OH), 1593 ν(C=N), 1153 ν(SO_2); ^{1}H-NMR (400MHz, DMSO-d^6); δ(ppm); 3.86 (3H,s,-OCH_3); 1.27 (3H,s,-CH_3); 2.65 (3H,t,-CH_3); 4.25 (2H,q,-CH_2); 12.96 (1H,s,-CH); 7.06-9.06 (8H,c,Ar-H); Elemental Analysis Found (%) C, 54.21; H, 4.17; N, 12.62; Calculated $C_{25}H_{23}N_5O_6S_2$ C, 54.24; H, 4.19; N, 12.65.

[$(L_2)_2MoO_2$]: M.F- $C_{50}H_{44}MoN_{10}O_{14}S_4$; yield 81%; M.W. 1233.16; Brown; Elemental Analysis Found (%) C, 48.67; H, 3.58; N, 11.33; Mo, 7.81; Calculated for $C_{50}H_{44}MoN_{10}O_{14}S_4$; C, 48.70; H, 3.60; N, 11.36; Mo, 7.78.

[$(L_2)_2WO_2$]: M.F- $C_{50}H_{44}N_{10}O_{14}S_4W$; Yield 83%; M.W. 1321.04; Red; Elemental Analysis Found (%) C, 45.44; H, 3.32; N, 10.58; W, 13.96 Calculated for $C_{50}H_{44}N_{10}O_{14}S_4W$; C, 45.46; H, 3.36; N, 13.60; W, 13.92.

[$(L_2)_2VO$]: M.F- $C_{50}H_{44}N_{10}O_{13}S_4V$; Yield 87%; M.W. 1172.15; Red; Elemental Analysis Found (%) C, 51.20; H, 3.74; N, 11.93; V, 4.39; Calculated for $C_{50}H_{44}N_{10}O_{13}S_4V$; C, 51.23; H, 3.78; N, 11.95; V, 4.35.

[$(L_2)_2ZrO$]: M.F- $C_{50}H_{44}N_{10}O_{13}S_4Zr$; yield 79%; M.W. 1212.43; Brown; Elemental Analysis Found (%) C, 49.51; H, 3.61; N, 11.53; Zr, 7.55; Calculated for $C_{50}H_{44}N_{10}O_{13}S_4Zr$; C, 49.53; H, 3.66; N, 11.55; Zr, 7.55.

Results and Discussion

NMR spectra of ligands: The experimental part contains the ^{1}H-NMR data for L_1 and L_2. The spectra of ligand L_1 show that the Ar-H is obtained as a complex peak in the aromatic region in the range of 6.37-8.91 δppm and the peak for the –OCH_3 proton is obtained as a singlet at 3.85 δppm, while the singlet for the –CH proton is obtained at 12.40 δppm. It can be seen from the ligand L_2 spectra that the proton for -OCH_3 has a singlet peak at 3.86 δppm. While the singlet for the -CH proton is produced at 12.96 δppm and the Ar-H are obtained as a complex peak in the aromatic region in the range of 7.06-9.06 δppm, the peak for the -CH_3 proton is acquired as a singlet at 1.27 δppm and the triplet quartet system is detected, confirming the presence of the -OCH_2CH_3 group. It is challenging to definitively attribute each signal to a specific aromatic, -NH, or -OH proton in the ^{1}H NMR spectra of both ligands since the signals of these protons were mixed with aromatic protons and were very tightly spaced out in the spectrum. Nonetheless, the number of protons precisely matches the compound's chemical formula, which was further supported by mass spectra.

Infrared spectra: The comparative IR data of rare earth transition metals with Schiff base ligands are shown in table 1. For identification purpose of binding mode of metal complexes and Schiff base ligands, the IR data were compared. The azomethine group's ν(C=N) is clearly observed as prominent band between 1577 cm^{-1} and 1593 cm^{-1} for Schiff base ligands. This band arises between 1546 cm^{-1} and 1563 cm^{-1} in coordination compounds; its lower energy shift depicts azomethine N coordination. The band for ν(SO_2) arises between 1151 cm^{-1} and 1153 cm^{-1} for ligands and band arises in between 1126 cm^{-1} and 1155 cm^{-1} for heterochelates.

Table 1
IR Data of Ligands and its Heterochelates

S.N.	Compound	C=N	OH	S=O	M-O	M-N	C=O
1	L1	1593	3360	1153	-	-	-
2	$[(L_1)_2MoO_2]$	1560	-	1155	524	605	-
3	$[(L_1)_2WO_2]$	1558	-	1130	557	614	-
4	$[(L_1)_2VO]$	1563	-	1126	549	617	-
5	$[(L_1)_2ZrO]$	1558	-	1153	549	607	-
6	L2	1577	3313	1151	-	-	1712
7	$[(L_2)_2MoO_2]$	1553	-	1153	554	638	1710
8	$[(L_2)_2WO_2]$	1546	-	1151	580	637	1710
9	$[(L_2)_2VO]$	1546	-	1151	578	638	1710
10	$[(L_2)_2ZrO_2]$	1551	-	1153	555	637	1710

Table 2
Ligands and metals electronic spectra and magnetic moments

S.N.	Compound	$\pi\rightarrow\pi^*$ λ_{max} (nm)	LMCT λ_{max} (nm)	$n\rightarrow\pi^*$ λ_{max} (nm)	d-d transition λ_{max} (nm)	μ (B.M.)	Chemical Shift
1	L1	257.8	274.4	354.6	-	-	-
2	$[(L_1)_2MoO_2]$	**257.6**	276.2	355	-	-	Hyperchromic
3	$[(L_1)_2WO_2]$	**258.7**	269.8	355.9 460	-	-	Hyperchromic
4	$[(L_1)_2VO]$	**259.6**	269	351	444	1.70	Hyperchromic
5	$[(L_1)_2ZrO]$	**257.6**	272	359 435.8	-	-	Hyperchromic
6	L_2	257.4	330.8	471.6	-	-	-
7	$[(L_2)_2MoO_2]$	**257.2**	278	332	468.6	-	Hyperchromic
8	$[(L_2)_2WO_2]$	**256.8**	334.4	471	-	-	Hyperchromic and Hypsochromic
9	$[(L_2)_2VO]$	**259**	275	336.2	457.6	1.69	Hypochromic and Hypsochromic
10	$[(L_2)_2ZrO]$	**257.6**	278.4	334.2473	-	-	Hyperchromic

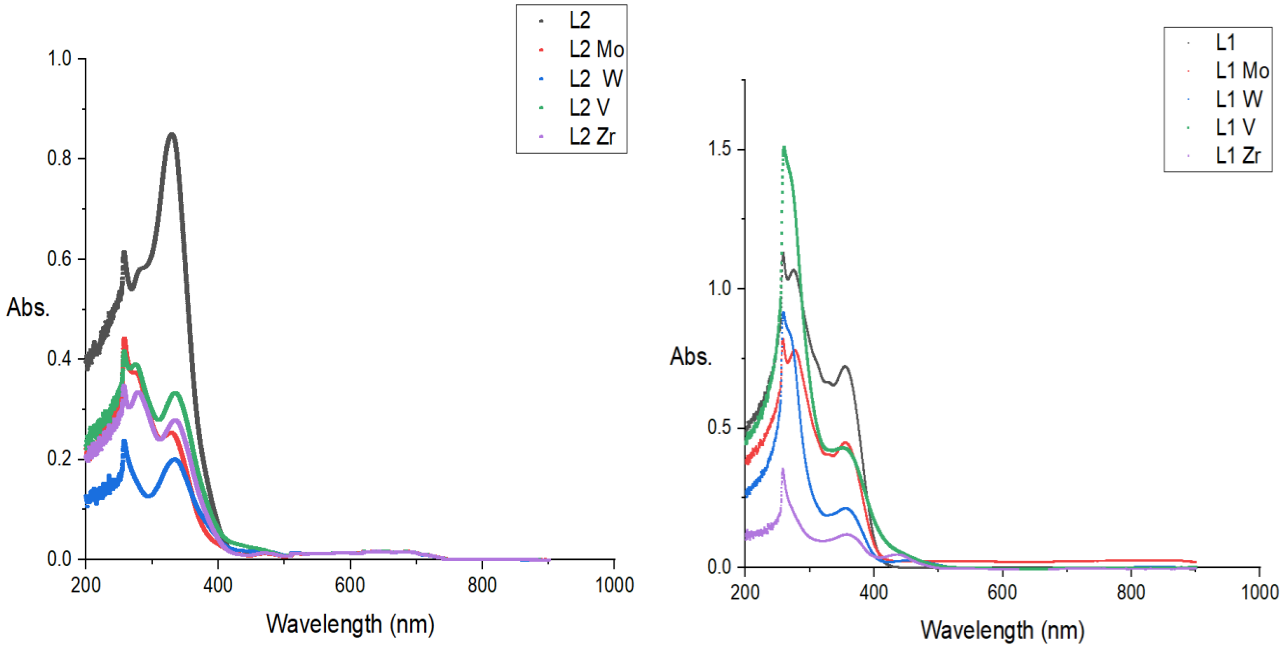

Figure 3: UV-Visible overlay spectrum of ligands (L_1, L_2) and their heterochelates

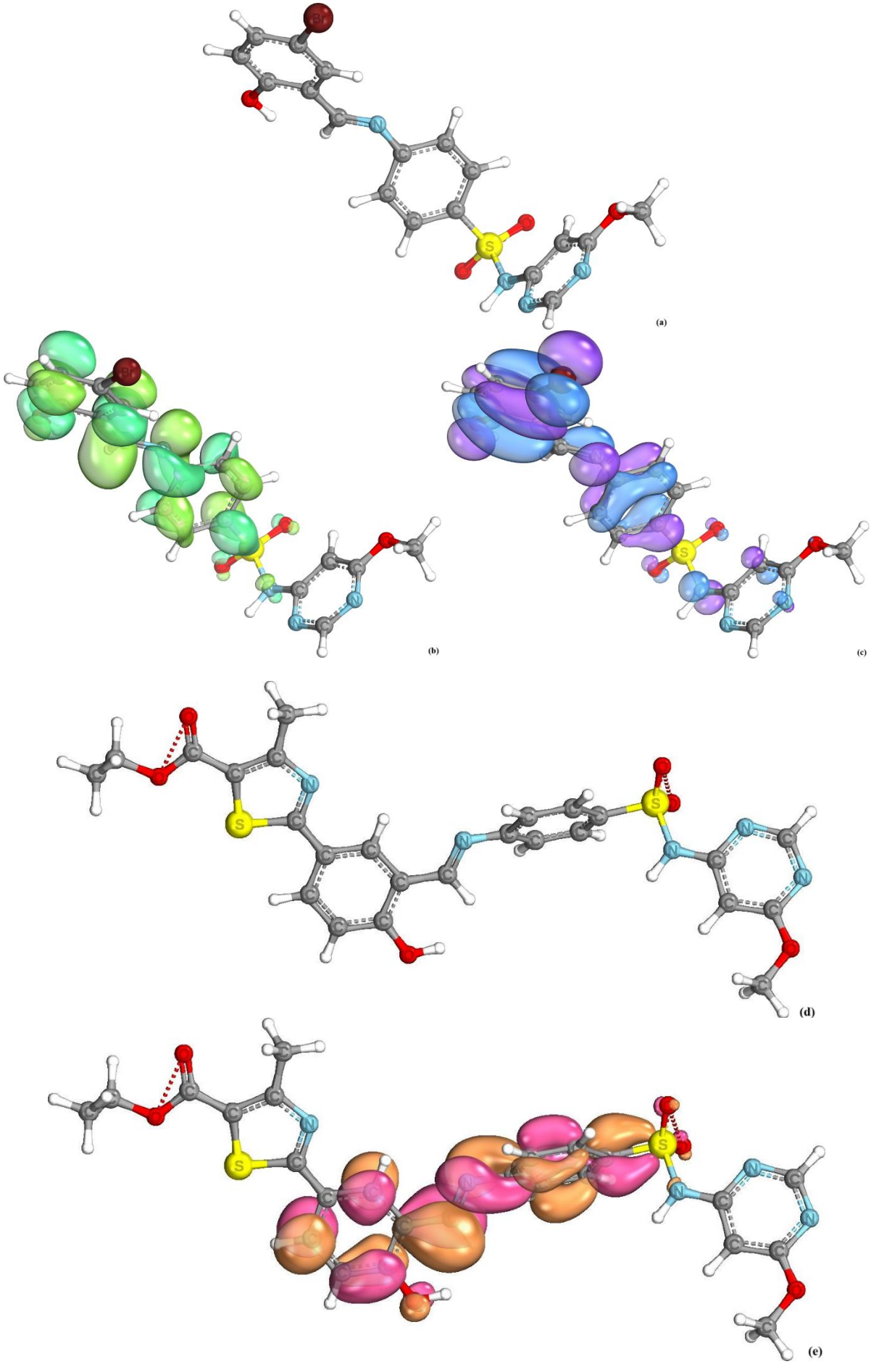
(a)
(b)
(c)
(d)
(e)

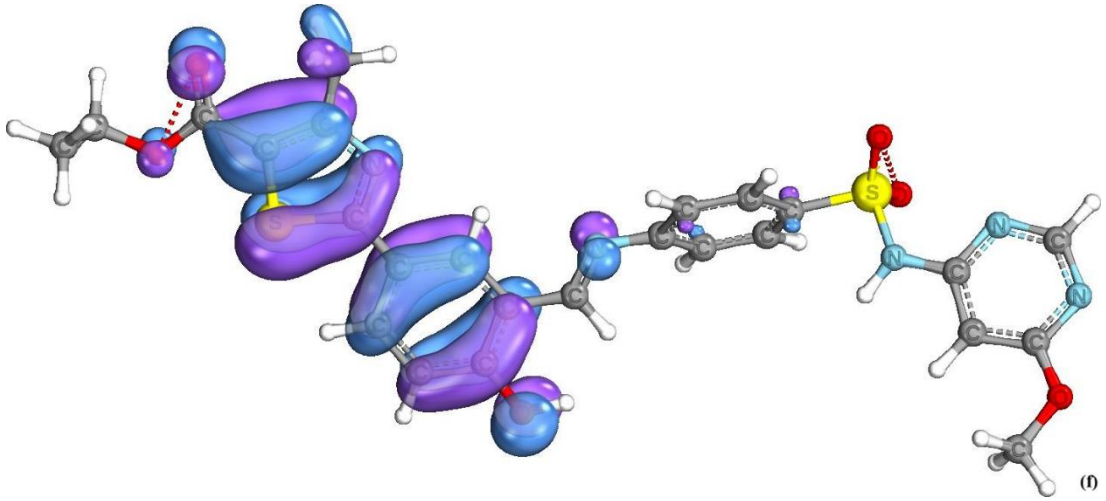

Figure 4: Electronic details of Ligand L_1 (a) Ligand L_1 after geometry optimization (b) Ligand L_1 HOMO (c) Ligand L_1 LUMO Electronic details of Ligand L_2 (d) Ligand L_2 after geometry optimization (e) Ligand L_2 HOMO (f) Ligand L_2 LUMO

UV-Vis spectra: The UV-Vis spectrum of the synthesized compound was recorded to analyse its electronic transitions and assess its optical properties. The absorption spectrum exhibited characteristic peaks at specific wavelengths mentioned in the table 2, corresponding to π→π*, n→π* or d-d transitions, indicating the presence of conjugated systems and lone pair interactions. The intensity and position of these peaks suggest metal-ligand charge transfer (MLCT) or other relevant effects. The heterochelate depicts shifts compared to corresponding ligand shown in table suggest possible, ligand coordination, or electronic environment. These findings validate the compound's successful production and structural soundness, providing insight into its electronic structure. Figure 3 depicts comparative UV-Visible overlay spectrum of ligands (L_1, L_2) and their heterochelates.

Computational studies: The electronic properties of ligand L_1, calculated using DFT at the def2-TZVP level, reveal a HOMO energy of -0.1293 eV and a LUMO energy of -0.2128 eV. Throughout the entire π-conjugated system, the HOMO and LUMO are widely delocalized, these def2-TZVP values contribute to a comprehensive understanding of Ligand L_1's electronic structure. Specifically, these energy levels support the observation that the substituent, present in Ligand L_1, acts as an electron-withdrawing group, influencing the HOMO and LUMO energies. For ligand L_2, DFT calculations at the def2-TZVPP level yielded a LUMO energy of -0.2201 eV and a HOMO energy of -0.1281 eV. The def2-TZVPP results further solidify the electronic characterization of ligand L_2, providing a consistent picture of its electronic structure. Figure 4 shows the details of respective ligands.

Molecular Docking studies: The RCSB protein data bank provided the crystal structure of the ternary complex of *E. coli* dihydropteroate synthetase (DHPS), PDB ID: 1AJ0. Water molecules and non-essential ligands were removed and check for missing residues if there. Polar hydrogens were added and appropriate charges were assigned using Auto-Dock Tools. The MMFF94 force field was used to optimize the ligand's three-dimensional structure, assigned Gasteiger charges and saved in PDBQT format for docking. A grid box was used to define the DHPS active site and Auto-Dock's Lamarckian genetic algorithm (LGA) was used for docking. Auto-Dock was used to do molecular docking simulations and the interaction profiles and docking scores were examined. RMSD (Root Mean Square Deviation) values were computed to evaluate docking reliability and known DHFR inhibitors were redocked to confirm binding modes in order to validate the docking results (Table 3).

All docking simulations were run under strictly regulated computational limitations, including high thresholds for genetic algorithm iterations, elitism settings and lengthy energy reduction cycles, in order to improve methodological rigor and guarantee maximum sampling fidelity. By methodically examining ligand flexibilities across torsional degrees of freedom, a structure with reduced internal strain and optimal steric complementarity to the active site topology of the enzyme was discovered. Simultaneously, the DHPS macromolecular architecture's electrostatic potential surface mappings informed by quantum mechanics clarified the hydrophobic microenvironments and heterogeneous charge distributions, supporting the spatial correlation of observed ligand-receptor affinities.

The presence of interactional hotspots and localized binding microdomains, controlled by complex steric, electrostatic and van der Waals complementarities, was demonstrated by subsequent post-docking topological reconstructions using molecular surface techniques and interactional heatmap matrices. The ligand frameworks demonstrated conformational rigidity and reduced entropic penalties because of their limited rotameric freedom, indicating a favorable binding enthalpy-driven mechanism, even though entropic contributions were not explicitly computed using thermodynamic integration or normal mode analysis.

Using molecular docking, the binding affinities of ligands and active residues in the protein's binding cavity were examined. Strong binding affinities were found by molecular docking experiments of ligands with DHPS. Projected binding energy values for ligand L_1 and ligand L_2 were -8.30 kcal/mol and -7.28 kcal/mol respectively, indicating a decent drug-protein interaction. The docking results are mentioned in table 3. Both ligands also interacted with protein via H-bond interactions, Ligand L_1 shows H-bonding interaction with ARG280 (2.068Å) amino acid and GLU150 (2.149 Å) for ligand L_2. LYS221, PHE190 and ARG63 contributed to hydrophobic interactions for ligand L_1 while HIS252 and HIS208 are responsible for hydrophobic interactions for ligand L_2 which stabilized the complex.

Furthermore, Phe190 amino acid shows T-shaped face to edge π-π staking interaction between thiazole and phenyl ring in ligand L_2. In addition to that amino acids ALA151, PRO64, LYS221 and ARG63 also take part in staking interaction. In ligand L_1 PRO15, LEU223 and LYS279 are involved in stacking interactions. The molecular docking interactions with ligands are shown in figure 5.

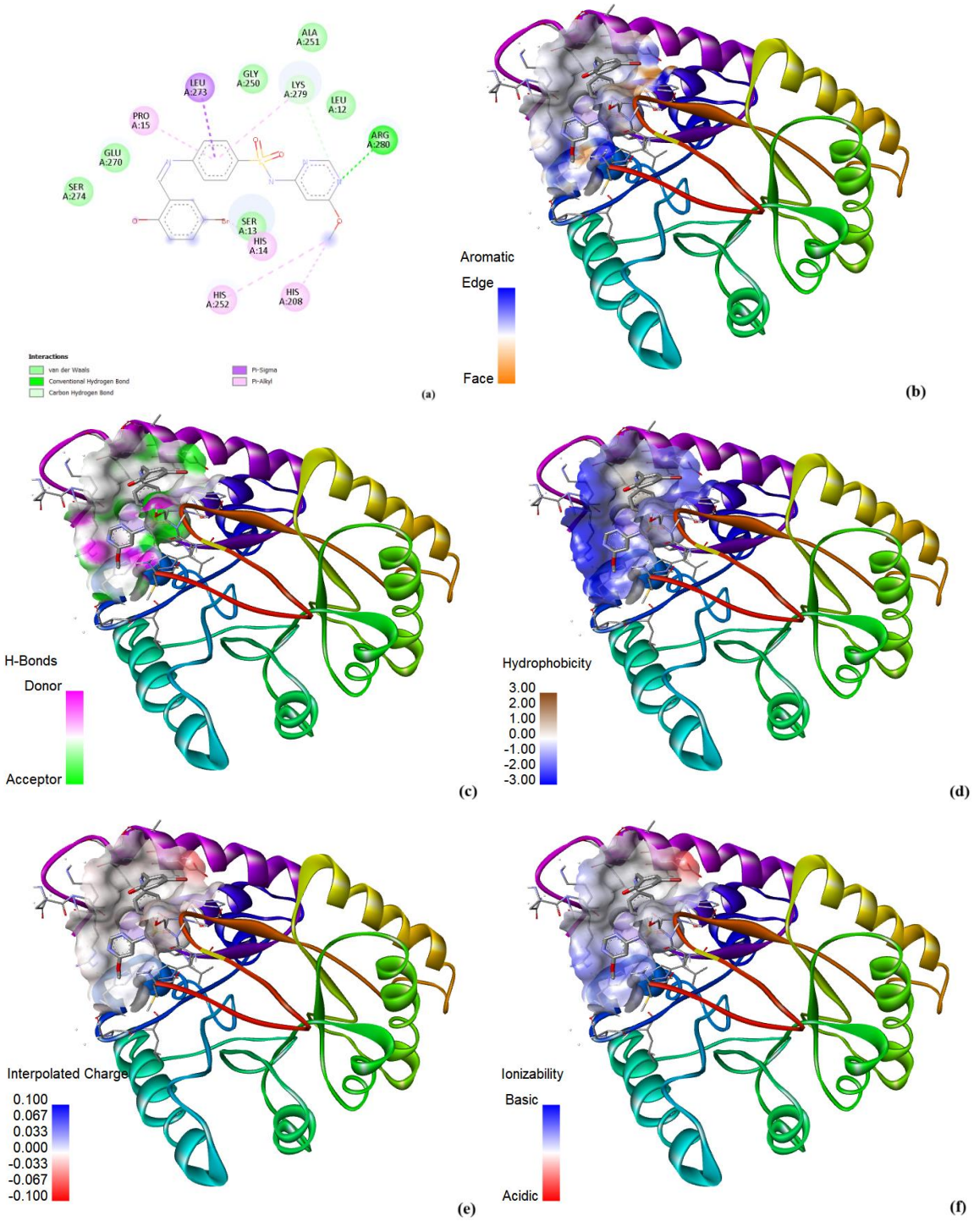

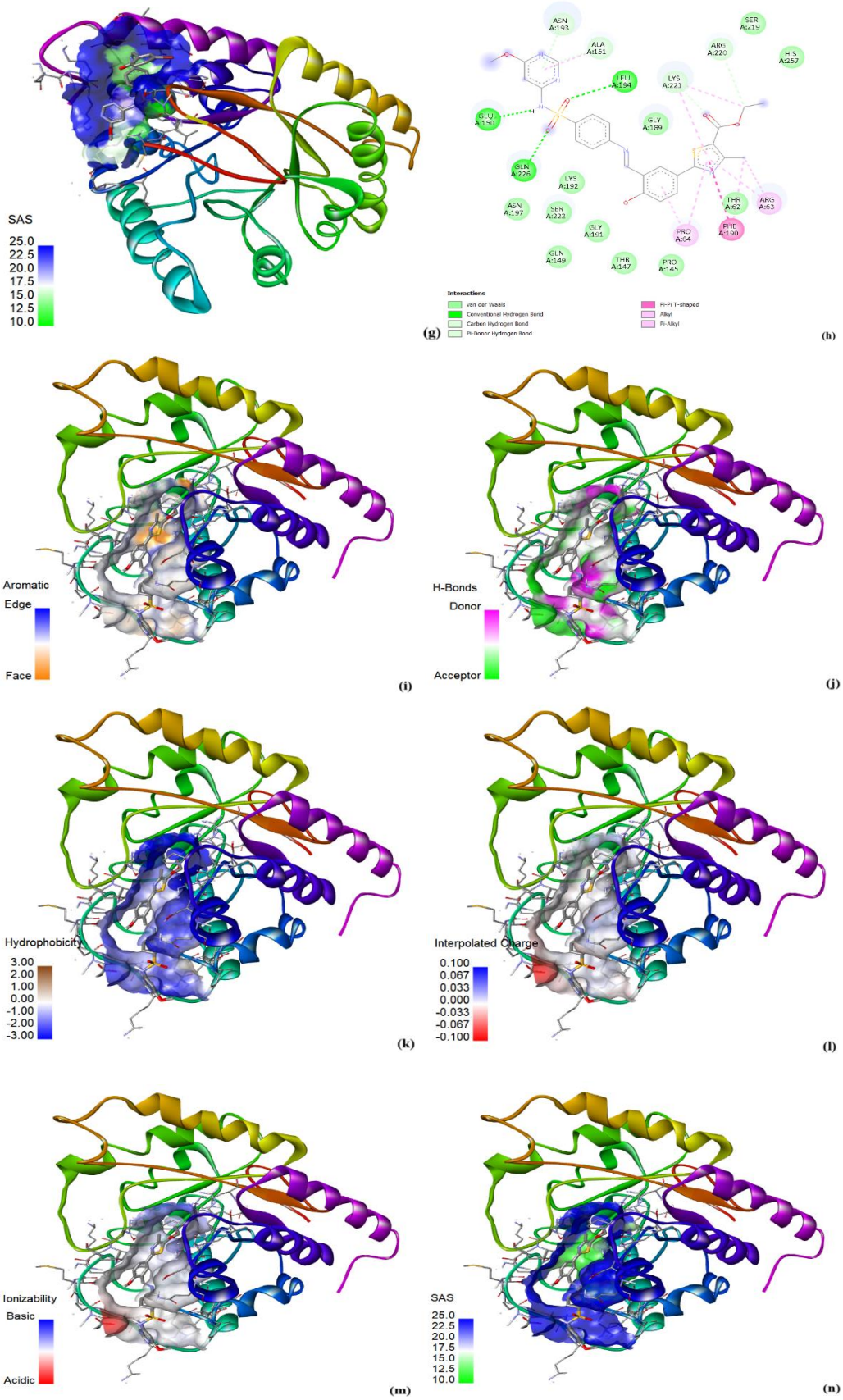

Figure 5: The molecular docking interaction images of ligand L_1 and L_2: (a) 2D Ligand interaction diagram (L_1), (b) Aromatic cavity (L_1), (c) H-bond cavity (L_1), (d) Hydrophobic cavity (L_1), (e) Interpolated charge cavity (L_1), (f) Ionizability cavity (L_1), (g) SAS cavity (L_1), (h) 2D Ligand interaction diagram (L_2), (i) Aromatic cavity (L_2), (j) H-bond cavity (L_2), (k) Hydrophobic cavity (L_2), (l) Interpolated charge cavity (L_2), (m) Ionizability cavity (L_2), (n) SAS cavity (L_2)

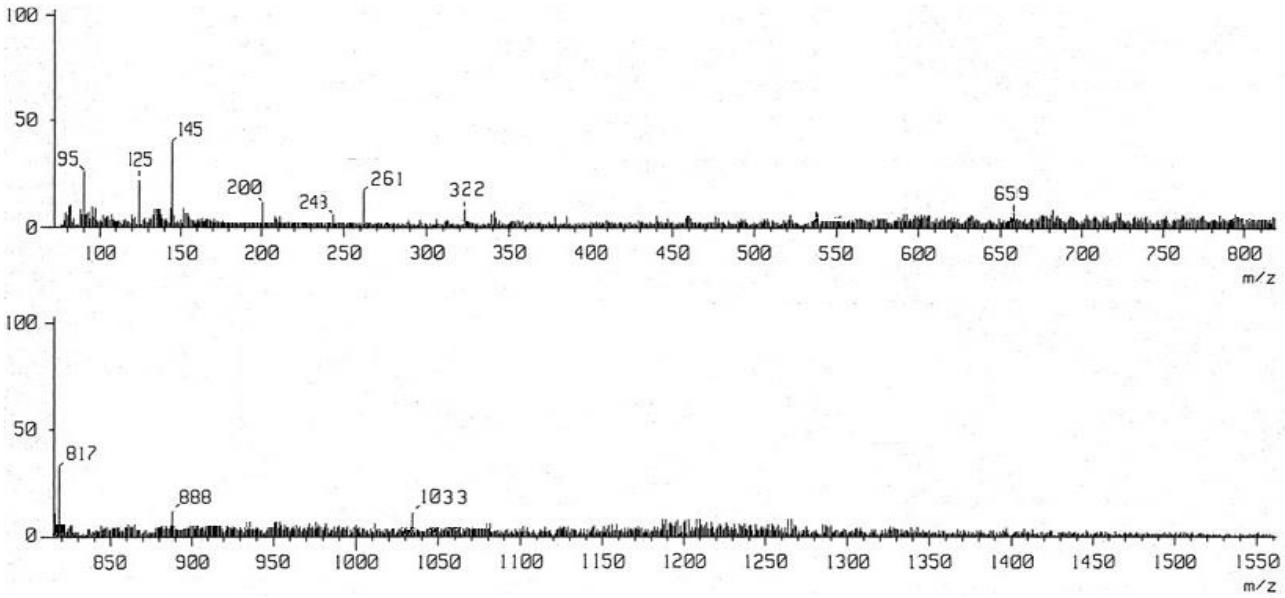

Figure 6: FAB mass spectrum for heterochelate $[(L_1)_2ZrO]$

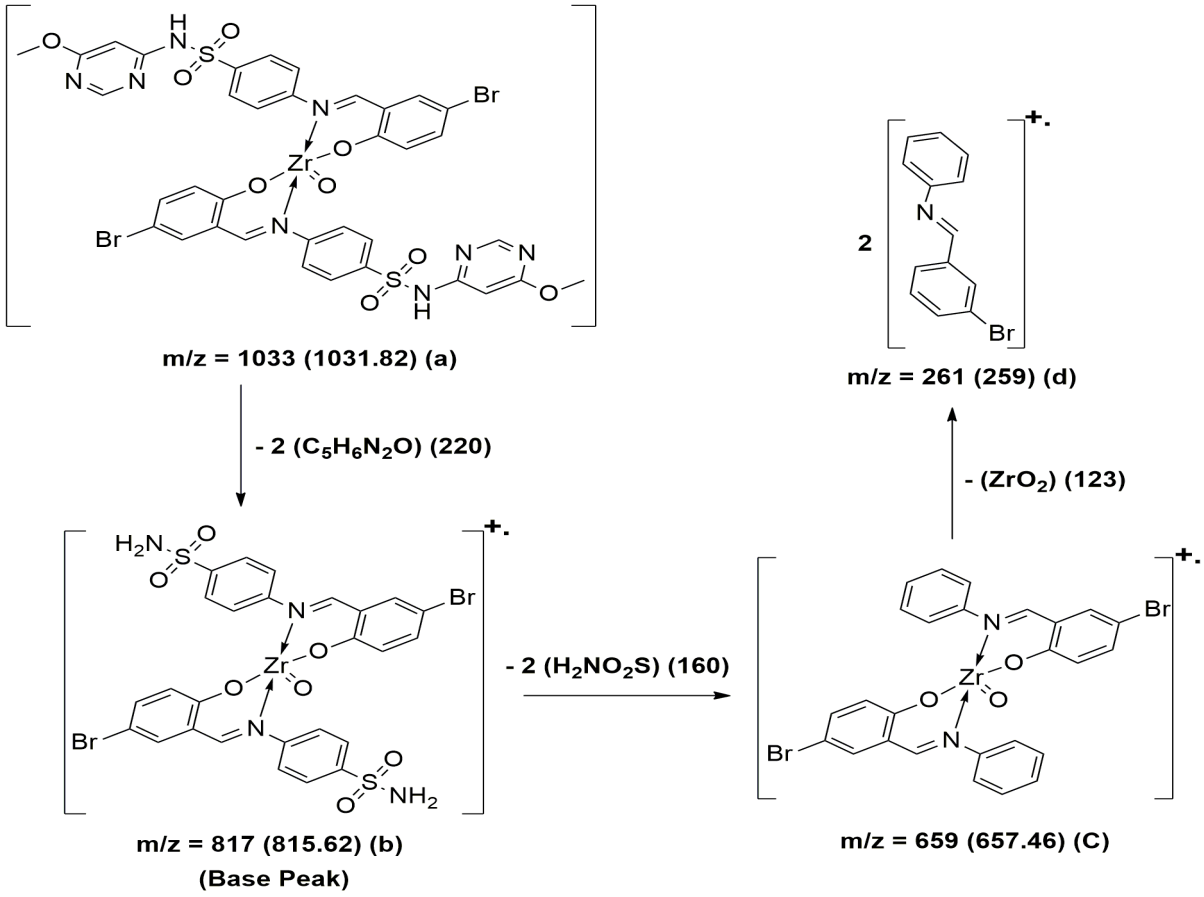

Figure 7: Fragmentation pattern of heterochelate $[(L_1)_2ZrO]$

Table 3
The Molecular Docking Analysis of synthesized Ligand with Protein

Protein	Ligands	RMSD	Binding energy (Kcal/mol)	Inhibition constant Ki
1aj0	L1	27.94	-8.30	879.66 nM
	L2	37.09	-7.28	4.63 µM

Table 4
Antibacterial properties of Ligand and its Heterochelates

S.N.	Compound	Gram positive		Gram negative		Fungi
		B.subtilus	*S.aureus*	*E.coli*	*P.aerugenosa*	*A.niger*
Reference Drug 1	Nystatin	NA	NA	NA	NA	22
Reference Drug 2	Streptomycin	28	29	24	22	NA
Solvent	DMSO	0	0	0	0	0
1	L1	0	10	15	2	0
2	$[(L_1)_2MoO_2]$	2	8	4	2	0
3	$[(L_1)_2WO_2]$	0	10	11	4	16
4	$[(L_1)_2VO]$	0	10	22	5	4
5	$[(L_1)_2ZrO]$	0	11	18	4	0
6	L2	17	15	14	6	0
7	$[(L_2)_2MoO_2]$	11	9	10	7	8
8	$[(L_2)_2WO_2]$	16	14	14	7	0
9	$[(L_2)_2VO]$	15	10	10	10	2
10	$[(L_2)_2ZrO_2]$	18	10	11	6	0

Collectively, these findings delineate a nuanced molecular interaction landscape and provide a foundational framework for future structure-based lead refinement and advanced quantum-chemical binding free energy evaluations.

FAB Mass: The molecular formula of the suggested chemical was verified using the validated mass spectra (Figure 6) and the molecular ion peak of the coordination molecule $[(L_1)_2ZrO]$. Figure 6 illustrates the trend of systematic fragmentation. The molecular ion peak initially appears at m/z=1033. The probable fragmentation pathway of the molecule is shown in figure 7. The compound's principal fragmentation results from the loss of a few of $C_5H_6N_2O$ molecules from species (a), giving rise to species (b), which has a prominent base peak at m/z=817. More fragmentation leads to species (c) by losing some of the ligand molecule (H_2NO_2S). Species (c) then undergoes further breakdown to produce a stable species (d), most likely due to the loss of the ZrO_2 and the remaining ligand molecule. All the calculated molecular weights agreed with the anticipated values from earlier research[26, 27].

Biological Screening: The synthesized Schiff base Ligands L_1 and L_2 and their heterochelates based on rare earth metals were screened against four bacterial stains *Bacillus subtilus, Staphylococcus aureus, E. coli, Pseudomonas aerugenosa* bacteria and fungi *Aspergillus niger*. Heterochelates exhibit a stronger inhibitory effect than their parent Schiff base ligands, as demonstrated in the antimicrobial screening results presented in table 4. Heterochelate $[(L_2)_2ZrO_2]$ is considerably affected against *Bacillus subtilus* and heterochelate $[(L_2)_2WO_2]$ and ligand L_2 is effective against *Staphylococcus aureus*.

Heterochelate $[(L_1)_2VO]$ is considerably effective against *E. Coli* and $[(L_2)_2VO]$ is moderately effective against *Pseudomonas aeruginosa*. $[(L_1)_2WO_2]$ heterochelate is considerably effective against fungi *Aspergillus niger*. The overtone notion[19,20] and chelation theory[39] can be used to describe the higher activity of heterochelates than the ligands.

Conclusion

We investigated the creation of novel Schiff base ligands from sulfa medication compounds and the heterochelates. We employed sophisticated methods such as ^{1}H-NMR, IR, UV and mass spectrometry for verification and characterization in order to guarantee the purity and structure of these compounds. The effectiveness of these chemicals in treating bacterial and fungal illnesses was carefully assessed when they were synthesized. The DFT simulations validate the impact of electron-withdrawing substituents on the HOMO and LUMO energies of ligands L_1 and L_2, offering a comprehensive understanding of their electronic characteristics.

Strong binding affinities of ligands L_1 and L_2 with DHPS are confirmed by molecular docking experiments, which are backed by substantial hydrophobic and hydrogen bonding interactions. Together with π-π stacking, these interactions support the stability of the ligand-protein complexes, underscoring their capacity for efficient binding. These ligands are attractive scaffolds for more logical drug design and optimization efforts targeting bacterial DHPS, highlighted by their structural and electrostatic complementarity as well as their low entropic penalties.

In contrast to Gram +ve bacterial strains like *B. subtilis* and *S. aureus*, as well as Gram -ve strains like *E. coli* and *P. aeruginosa*, the coordination compounds showed notable antibacterial characteristics and pronounced activity. Compared to their separate ligands, their antibacterial actions were really substantially stronger. These results are intriguing because they raise the possibility that these substances could be studied further and turned into a new

class of antibacterial medications based on transition metals that could combat a variety of dangerous microorganisms.

References

1. Alves B.R., Da Silva C.M., Da Silva D.L., Modolo L.V. and De Resende A.M., Schiff bases: A short review of their antimicrobial activities, *J. of Adv. Research*, **2(1)**, 1-8 **(2011)**

2. Axelrod L., Cryer E.P., Grossman A.B., Heller S.R., Montori V.M., Seaquist E.R. and Service F.J., Evaluation and management of adult hypoglycemic disorders: an Endocrine Society Clinical Practice Guideline, *The Journal of Clinical Endocrinology & Metabolism*, **94(3)**, 709-728 **(2009)**

3. Bala S., Kajal A., Kamboj S., Saini V. and Sharma N., Schiff bases: a versatile pharmacophore, *J. of Catalysts*, **2013(1)**, 893512 **(2013)**

4. Barboiu C.T., Brewster E., Dinculescu M.E., Luca M. and Pop C., Carbonic anhydrase activators, part 14: syntheses of mono and bis pyridinium salt derivatives of 2-amino-5-(2-aminoethyl)-and 2-amino-5-(3-aminopropyl)-1, 3, 4-thiadiazole and their interaction with isozyme II, *Eur. J. Med. Chem*, **31**, 597-606 **(1996)**

5. Biondi S., Long S., Panunzio M. and Qin W., Schiff bases: A short survey on an evergreen chemistry tool, *Molecules*, **18(10)**, 12264-12289 **(2013)**

6. Buchta V., Krátký M., Stolaříková J., Trejtnar F., Vinšová J. and Volková M., Antimicrobial activity of sulfonamides containing 5-chloro-2-hydroxybenzaldehyde and 5-chloro-2-hydroxybenzoic acid scaffold, *Eur. J. of Med. Chemistry*, **50**, 433-440 **(2012)**

7. Carradori S., Guglielmi P., Luisi G. and Secci D., Nitrogen-and Sulfur-Containing Heterocycles as Dual Anti-oxidant and Anti-cancer Agents, Handbook of Oxidative Stress in Cancer: Mechanistic Aspects, 2571-2588 **(2022)**

8. Carradori Simone et al, Nitrogen-and Sulfur-Containing Heterocycles as Dual Anti-oxidant and Anti-cancer Agents, Handbook of Oxidative Stress in Cancer: Mechanistic Aspects, Singapore, Springer Nature, Singapore, 2571-2588 **(2022)**

9. Carta F. et al, Ureido-substituted benzenesulfonamides potently inhibit carbonic anhydrase IX and show antimetastatic activity in a model of breast cancer metastasis, *J. Med. Chem.*, **54**, 1896–1902 **(2011)**

10. Casini A., Scozzafava A. and Supuran C.T., Protease inhibitors of the sulfonamide type: anticancer, antiinflammatory and antiviral agents, *Medicinal Research Reviews*, **23(5)**, 535-558 **(2003)**

11. Chohan H.Z., Hadda B.T., Jarrahpour A. and Youssoufi H.M., Identification of antibacterial and antifungal pharmacophore sites for potent bacteria and fungi inhibition: indolenyl sulfonamide derivatives, *Eur. J. of Med. Chem.*, **45(3)**, 1189-1199 **(2010)**

12. Chohan H.Z., Scozzafava A. and Supuran C.T., Metalloantibiotics: synthesis and antibacterial activity of cobalt (II), copper (II), nickel (II) and zinc (II) complexes of kefzol, *J. of Enzyme Inhibition and Med. Chem.*, **19(1)**, 79-84 **(2004)**

13. Chohan H.Z. and Shad A.H., Structural elucidation and biological significance of 2-hydroxy-1-naphthaldehyde derived sulfonamides and their first-row d-transition metal chelates, *J. of Enzyme Inhibition and Medicinal Chemistry*, **23(3)**, 369-379 **(2008)**

14. Chohan H.Z., Synthesis and Biological Properties of Cu (II) Complexes with 1, 1′-Disubstituted Ferrocenes, *Synthesis and Reactivity in Inorganic and Metal-organic Chemistry*, **34(5)**, 833-846 **(2004)**

15. Chohan H.Z., Hadda B.T., Shad A.H. and Youssoufi H.M., Some new biologically active metal-based sulfonamide, *Eur. J. of Med. Chem.*, **45(7)**, 2893-2901 **(2010)**

16. Cooper D.S. and Laurberg P., Hyperthyroidism in pregnancy, *The Lancet Diabetes & Endocrinology*, **1(3)**, 238-249 **(2013)**

17. Demir E.N., Kiraz A., Mestav B.U., Tan E., Ünver H., Yıldırım N. and Yıldız M., Synthesis and spectral, antimicrobial, anion sensing and DNA binding properties of Schiff base podands and their metal complexes, *Rus. J. of General Chemistry*, **85**, 2149-2162 **(2015)**

18. Dong Z., Guo B., Huang H., Jia B., Lu Y., Ren X., Wang W., Zhao X. and Zhou S., Degradable biomedical elastomers: paving the future of tissue repair and regenerative medicine, *Chem. Society Reviews*, **53(8)**, 4086-4153 **(2024)**

19. El-Metwaly M.N., Spectral and biological investigation of 5-hydroxyl-3-oxopyrazoline 1-carbothiohydrazide and its transition metal complexes, *Transition Metal Chem.*, **32(1)**, 88-94 **(2007)**

20. Gajera P., Parmar R. and Vadodaria M., Transition metal-based coordination compounds of Schif f base derived from drug molecules: Synthesis, spectroscopic and *in vitro* biological screening, *Ind. J. of Chem.*, **63**, 992-998 **(2024)**

21. Ge H.M., Li H.Q., Shi L., Song C.Y., Tan R.X., Tan H.S. and Zhu H.L., Synthesis and antimicrobial activities of Schiff bases derived from 5-chloro-salicylaldehyde, *Eur. J. of Med. Chem.*, **42(4)**, 558-564 **(2007)**

22. Govindaraj V. and Ramanathan S., Synthesis, spectral characterisation, electrochemical and fluorescence studies of biologically active novel Schiff base complexes derived from E-4-(2-hydroxy-3-methoxybenzlideneamino)-N-(pyrimidin-2-yl) benzenesulfonamide, *Turkish J. of Chem.*, **38(4)**, 521-530 **(2014)**

23. Griffith C.E., Wallace J.M., Wu Y., Kumar G., Gajewski S., Jackson P., Phelps A.G., Zheng Z., Rock C.O., Lee E.R. and White S.W., The structural and functional basis for recurring sulfa drug resistance mutations in *Staphylococcus aureus* dihydropteroate synthase, *Frontiers in Microbiology*, **9**, 136 **(2018)**

24. Gupta A. and Halve A.K., [Beta]-lactams: A mini review of their biological activity, *Int. J. of Phar. Sci. and Research*, **6(3)**, 978 **(2015)**

25. Hadi Ameer Mezher, Alfatlawi Wael Rasheed and Hameed Ahmed Shandookh, A study of some physiological parameters in patients previously infected with COVID-19, *Res. J. Biotech.*, **19(11)**, 1-6 **(2024)**

26. Jani D.H., Keharia H., Modi C.K. and Patel H.S., Novel drug-based Fe (III) heterochelates: synthetic, spectroscopic, thermal and

in-vitro antibacterial significance, *App. Organomet. Chem.*, **24(2)**, 99-111 **(2010)**

27. Jani D.H. and Modi C.K., Mn (III) mixed-ligand complexes with bis-pyrazolones and ciprofloxacin drug: synthesis, characterization and antibacterial activities, *App. Organomet. Chem.*, **25(6)**, 429-436 **(2011)**

28. Mandal M.S., Mondal S., Mondal K.T. and Sinha C., Spectroscopic characterization, antimicrobial activity, DFT computation and docking studies of sulfonamide Schiff bases, *J. of Mol. Structure*, **1127**, 557-567 **(2017)**

29. Menabuoni L., Scozzafava A., Mincione F., Briganti F., Mincione G. and Supuran C.T., Carbonic anhydrase inhibitors. Water-soluble, topically effective intraocular pressure lowering agents derived from isonicotinic acid and aromatic/heterocyclic sulfonamides: is the tail more important than the ring?, *J. Enzyme Inhib. Med. Chem.*, **14(6),** 457-474 **(1999)**

30. Mustafa M. and Winum J.Y., The importance of sulfur-containing motifs in drug design and discovery, *Expert Opinion on Drug Discovery*, **17(5)**, 501-512 **(2022)**

31. Muthukumar R., Karnan M., Elangovan N., Karunanidhi M. and Thomas R., Synthesis, spectral analysis, antibacterial activity, quantum chemical studies and supporting molecular docking of Schiff base (E)-4-((4-bromobenzylidene) amino) benzenesulfonamide, *J. Indian Chem. Soc.*, **99(5)**, 100405 **(2022)**

32. Parkkila S., Pastorek J., Pastorekova S. and Supuran C.T., Carbonic anhydrases: current state of the art, therapeutic applications and future prospects, *J. of Enzyme Inhibition and Medicinal Chemistry*, **19(3)**, 199-229 **(2004)**

33. Patrick G.L., An introduction to medicinal chemistry, Oxford University Press **(2023)**

34. Pastorekova S., Vullo D., Casini A., Scozzafava A., Pastorek J., Nishimori I. and Supuran C.T., Carbonic anhydrase inhibitors: Inhibition of the tumor-associated isozymes IX and XII with polyfluorinated aromatic/heterocyclic sulfonamides, *J. Enzyme Inhib. Med. Chem.*, **20(3)**, 211-217 **(2005)**

35. Ricci F., Bonham A.J., Mason A.C., Reich N.O. and Plaxco K.W., Reagentless, electrochemical approach for the specific detection of double-and single-stranded DNA binding proteins, *Analytical Chemistry*, **81(4)**, 1608-1614 **(2009)**

36. Stepnicka P., ed., Ferrocenes: From Materials and Chemistry to Biology, Wiley **(2008)**

37. Supuran C.T., Diuretics: from classical carbonic anhydrase inhibitors to novel applications of the sulfonamides, *Current Pharmaceutical Design*, **14(7)**, 641-648 **(2008)**

38. Supuran C.T., Carbonic anhydrases: novel therapeutic applications for inhibitors and activators, *Nature Reviews Drug Discovery*, **7(2)**, 168-181 **(2008)**

39. Tweedy B.G., Plant extracts with metal ions as potential antimicrobial agents, *Phytopathology*, **55(8)**, 910-914 **(1964)**

40. Werth B.J. and Pharm D., University of Washington School of Pharmacy, Introducción a los antibióticos **(2022)**.

(Received 21st April 2025, accepted 24th June 2025)